Defects Density of States Model of Cathodoluminescent Intensity and Spectra of Disordered SiO_2

Amberly Evans Jensen and J. R. Dennison, *Member, IEEE*

***Abstract*— Electron beam measurements show that disordered SiO_2 exhibits electron-induced luminescence, and that it varies with incident beam energy and current density, sample temperature, and wavelength. A simple model based on the electronic band structure and defect density of states—initially used to explain electron transport in highly disordered insulating materials—has been extended to predict the relative cathodoluminescent intensity and spectral radiance for disordered SiO_2 as a function of these variables. Due to the large band gap of insulating SiO_2, thermal excitation from the valence to conduction band is highly improbable; excitation is through collisions of the incident high energy electrons. For visible and near-IR (NIR) light to be emitted, there must be other states within the forbidden band gap for electrons to occupy. These localized defect or "trap" states of disordered SiO_2 are due to structural or substitutional chemical defects. Results for both thin film samples with penetrating radiation and thick bulk samples with nonpenetrating radiation are presented. The data were fit with the proposed model using saturation dose rate and mean shallow trap energy as fitting parameters, which compares favorably with results from independent experiments.**

***Index Terms*— cathodoluminescence, light emission, materials testing, space environment effects, low temperature**

I. Introduction

Because spacecraft reside in the harsh space plasma environment, there is a critical need to understand spacecraft charging due to the accumulation of an electrical charge on orbiting spacecraft induced by the space plasma environment [1]. These have harmful effects on spacecraft, causing more than half of all spacecraft anomalies attributed to the environment [2]. In addition to charging induced by space plasma fluxes, incident electrons can also generate light emission, termed cathodoluminescence. This can potentially produce a stray light background in space-based astronomical observatories which are exposed to high energy electron fluxes from space plasmas. The magnitude of cathodoluminescence will be significantly affected by the environmental conditions, in particular temperature and the energy spectrum and flux of impacting electrons. Energy spectra of severe space weather environments (*e.g.*, LEO, GEO, auroral, magnetosphere, and solar wind; see [2] or [3] and references therein) have on the order 10 μW-cm^{-2} incident electron power (*e.g.*, 10 nA-cm^{-2} at 1 keV or 1 nA-cm^{-2} at 10 keV); this provides an absolute scale for comparison of luminescent intensities observed in the experiments described here with extreme space effects. In the case of IR observatories or sensors, the applications often require low temperatures down to 10's of Kelvin.

The objective of this study was to investigate cathodoluminescence of a common optical material, disordered silicon dioxide, under simulated space plasma conditions, using laboratory conditions in a space simulation chamber [4,5]. Measurements were made of the absolute spectral radiance and optical emission spectra of this material, to quantify the effects of electron energy, current density and power density, temperature and sample thickness. Tests were conducted on two types of disordered SiO_2 samples: a thin optical coating on a reflective mirror with penetrating radiation and a thick bulk sample with nonpenetrating radiation. Absolute spectral radiance and emission spectra were measured over the full visible range and sample temperatures were varied from ~295 K to 40 K.

II. Experimentation

These experiments were conducted in the main USU ultrahigh vacuum electron emission test chamber [6], modified for observations of low intensity ultraviolet/visable/near infrared (UV/VIS/NIR) glow over a broad range of sample temperatures [5,7]. Experimentation—including electron sources, light detection instruments, cooling capabilities and sample preparation—is detailed further in [3-9].

Two monoenergetic electron sources were used, a low energy electron gun (20.0±0.5 eV to 5000±2 eV at ~50 pA-cm^{-2} to 1 μA-cm^{-2} [7] and a high energy gun (5.00 to 30.00±0.01 keV at ~50 pA-cm^{-2} to 1 μA-cm^{-2} [3]). Light detection used two *ex situ* cameras [8], calibrated for NIST-tracable absolute intensity measurements [5]; a Single Lens Reflex (SLR) CCD camera [~400 nm to 700 nm at 30 s shutter speeds with an average spectral response of ~$4\cdot10^9$ counts/(W/cm^2·sr·μm)] and an image-intensified CCD video camera [~400 nm to 900 nm at 30 frames/s with an average spectral response of ~$4\cdot10^{10}$ counts/(W/cm^2·sr·μm)] [9]. UV/Visible spectra were measured with a fiber optics-based

Research was supported by funding from the NASA Goddard Space Flight Center, the Air Force Research Laboratory through a National Research Council Senior Research Fellowship (Dennison), and a NASA Space Technology Research Fellowship (Jensen).

Amberly Evans Jensen and JR Dennison are with the Materials Physics Group in the Physics Department at Utah State University in Logan, UT 84322 USA. (e-mails: Amb.Eva@aggiemail.usu.edu and JR.Dennison@usu.edu)

Color versions of one or more figures in this paper are available online at http://ieeexplore.ieee.org.

Digital object identifier .

spectrometer [~250 nm to 1080 nm with ~1 nm resolution at ~65 s integration time] [10] with a MgF_2 window and *ex situ* collection optics [8,9].

Two sample cooling methods were used, a liquid N_2 reservoir from ~150-400 K with a stability of ±4 K maintained over typical 2 hr experiment durations [4] and a closed-cycle helium cryostat from <40-450 K ±0.5 K [5].

Two types of disordered SiO_2 samples were tested. The first sample type had a thin film (~60 nm thick) coating deposited on a gold-coated, optically flat mirror surface using plasma vapor depositon. The second sample type was a bulk sample, ~80 µm thick, made by traditional glass formation methods. The samples were optically cleaned and underwent a ~12 hr vacuum bakeout at ~390 K and $<1\cdot10^{-3}$ Pa to eliminate adsorbed water and volatile contaminates. The samples were mounted and placed in an ultrahigh vacuum chamber (base pressure $<1\cdot10^{-6}$ Pa) for >24 hr to allow for outgassing before measurements were made.

III. Cathodoluminescence Model

A model for the cathodoluminescence for highly disordered insulating materials has been developed by Jensen and Dennison, based on band models of the localized disordered trap states found in the forbidden band gap region of insulating materials [8,11]. It is an extension of theories for both band structures of defects states in crystalline materials [12,13] and luminescence in atomic and crystalline materials [14]. The overall luminescent intensity, I_γ, is proportional to the number of available states and the transition rates of each phase depicted in the modified Joblonski diagram [14,15] of Figure 1. Incident high energy electrons excite electrons from the valence band (VB) into the conduction band (CB); these are quickly trapped in shallow trap (ST) states just below the CB edge. These electrons in ST states can decay into deep level traps and emit luminescence photons.

The model predicts that I_γ scales with incident current density, J_b, incident beam energy, E_b, temperature, T, and emitted photon wavelength, λ, as

$$I_\gamma\left(J_b,E_b,T,\lambda;\varepsilon_{ST},\dot{D}_{sat}\right) \propto \left[\frac{\dot{D}(J_b,E_b)\dot{D}_{sat}}{\dot{D}(J_b,E_b)+\dot{D}_{sat}}\right]\rho_m\ Q_{e\gamma}(\lambda,T)\left[1-e^{-(\varepsilon_{ST}/k_BT)}\right] \times\begin{cases} R(E_b) & ;\ 0\le R(E_b)\le L, \quad \text{nonpenetrating} \\ L & ;\ 0\le L\le R(E_b), \quad \text{penetrating}\end{cases}, \quad (1)$$

where q_e is the electron charge, ρ_m is the mass density of the material, and $Q_{e\gamma}$ is the average conversion efficiency of excited electrons to photons (of various wavelengths). The overall intensity scales as the fraction of occupied ST (see thermal dependence below) and the number of unoccupied DT states (see Sec IV.D). Overall $Q_{e\gamma}$ is reduced by the fractions of CB, ST and DT electrons which can undergo non-radiative processes leading to recombination with holes in the VB or hole trap states. In equilibrium there are relatively few electrons in the CB as compared to ST, so CB recombination has minimal effect on $Q_{e\gamma}$. Since all other processes depicted in Fig. 1 originate from ST electrons, all bands scale equally with the number of occupied ST.

The penetration depth or range, $R(E_b)$, is an energy-dependent material property [16]. When the range is less than the sample thickness L, the beam is nonpenetrating and all the incident power is absorbed in the material. Penetrating radiation occurs when the range is greater than the sample thickness; here the absorbed power is reduced by a factor of $[L/R(E_b)]$ [8]. (See Appendix for further details.)

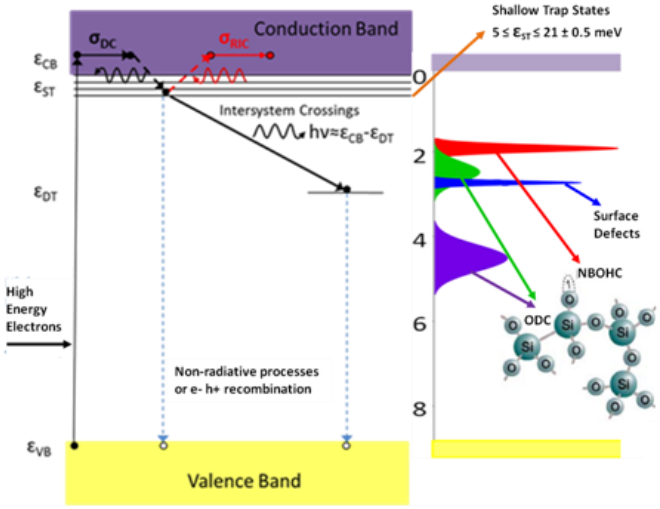

Band	Peak	Peak	FWHM	Defect	Ref.
Red	1.93±0.01 eV	663±3 nm	42 nm	NBOHC	[16,20,23]
Green	2.48±0.03	506±7	68	ODC	[17,23]
Blue	2.76±0.03	450±5	11	Surface	[18-20,23]
UV	4.97	275	50	ODC	[17-20,23]

Fig. 1. Modified Joblonski diagram for cathodoluminescence. Shown are transitions between the extended state valence (VB) and conduction (CB) bands, shallow trap (ST) states at ε_{ST} within ~k_BT below the CB edge, and deep trap (DT) distributions centered at ε_{DT}. Energy depths are exaggerated for clarity. The diagram at right depicts the approximate energy depths, widths and magnitudes of the four observed bands and their defect origins; values are listed in the table.

The dose rate (absorbed electron power per unit mass), $\dot{D}$, in a sample volume ($R(E_b)$ time the beam area) is given by

$$\dot{D}(J_b,E_b) = \frac{E_b\,J_b}{q_e\rho_m\,R(E_b)}[1-\eta(E_b)]\ . \quad (2)$$

Inclusion of a weakly energy-dependent backscatter coefficient, $\eta(E_b)$, in Eq. (2) corrects the dose rate for incident electrons that quasi-elastically backscatter without depositing appreciable energy in the material [8]. For the most part, this correction is small and weakly dependant on energy. For SiO_2, η is ~0.2 over the energies used here.

For biased samples, or when excess charge is stored in the trap states, a surface voltage V_s results and E_b is replaced everywhere in Eqs. (1) and (2) by the landing energy, $(E_b - q_eV_s)$. Thus, cathodoluminescence intensity may diminish appreciably for kV surface potentials often observed both on GEO satellites in eclipse and when samples charge in laboratory experiments [17]. In the calculations presented here, this affect was assumed to be negligible.

At high dose rates saturation is observed, characterized by a material and sample dependent saturation dose rate, $\dot{D}_{sat}$. At $\dot{D} \gg \dot{D}_{sat}$, the dose rate term in Eq. (1) approaches unity. When $\dot{D} = \dot{D}_{sat}$, the term equals 1/2; that is, $I_\gamma(\dot{D}_{sat})/I_\gamma(\dot{D} \gg \dot{D}_{sat})$= 1/2. At $\dot{D} \ll \dot{D}_{sat}$, $I_\gamma \propto \dot{D}_{sat}$. This is consistent with standard saturation models, including those for luminescence [8,14]. For example, similar suppression of I_γ can result from

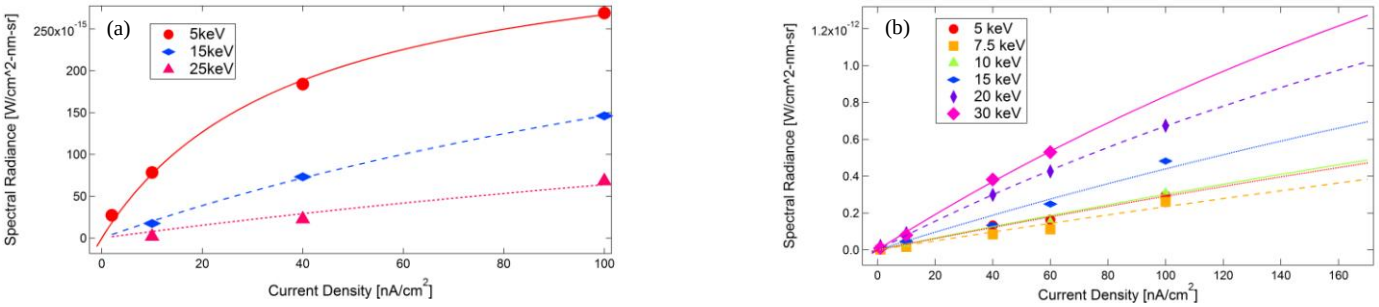

Fig. 2. Spectral radiance as a function of beam current density for various incident electron energies. (a) For the ~60 nm thick sample of SiO_2, penetration occurs at ~1.3 keV beam energy. The fits yield a value for $\dot{D}_{sat}$ of $4.4 \cdot 10^3 \pm 44\%$ Gy/s. (b) For the ~80 μm thick sample of SiO_2, penetration occurs at ~118 keV beam energy. The fits yield a value for $\dot{D}_{sat}$ of 577 ± 25% Gy/s.

a modified Stern-Volmer process for quenching due to non-radiative excited state reactions of the ST, where the ratio of quenched to unquenched emission is equal the ratio of unquenched-to-quenched lifetimes, $I_Q/I_o = \tau_o/\tau_Q = 1 + k_Q \tau_o n_Q$ [14]. One such reaction occurs when electrons in ST are thermally excited to the CB, leading to radiation induced conductivity (RIC, σ_{RIC}) in the presence of an electric field. RIC is complimentary to luminosity [12], with $\tau_Q \equiv k_Q n_Q \propto \sigma_{RIC} = k_{RIC}(T)\dot{D}^{\Delta(T)}$ [10]. When RIC is the only quenching reaction, a simple temperature-dependent model for the k_{RIC} and Δ parameters for dielectric materials [10] leads to $I_\gamma \propto \left[1 - e^{-(\varepsilon_{ST}/k_B T)}\right]$ with $\varepsilon_{ST} > k_B T$ equal to the minimum energy depth of the occupied ST states below the CB edge.

The thermal dependence of the overall luminescence is largely determined by ε_{ST}. In equilibrium, the vast majority of electrons excited into the CB by the high energy electrons are quickly trapped in ST, though some are thermally re-excited into the CB as RIC electrons. I_γ is proportional to the fraction of electrons that are retained in the ST and not thermally excited into the CB; that is, $I_\gamma \propto \left[1 - e^{-(\varepsilon_{ST}/k_B T)}\right]$. Retention times in the localized ST are much longer than the retention times for extended CB states, even at room temperature; therefore, the equilibrium population in the ST is much larger than in the CB. Thus, the number of electrons available for radiative relaxation into the DT states contributing to CL is less at higher temperatures. See Appendix VI.D for a discussion of additional temperature dependences for individual band intensities.

IV. Results

The measured absolute cathodoluminescent intensity of the disordered SiO_2 films [17] agreed within ~25% with previous measurements [18]. The measured dependence of spectral radiance on $J_b, E_b,$ and T and the emission spectra are described below. Fits to the data determine values of ε_{ST}, and $\dot{D}_{sat}$ and details about the band structure of disordered SiO_2.

A. Incident Beam Current Density and Saturation

For SiO_2 (band gap≈8.9 eV), excitation from the VB to CB is not thermal, but rather occurs through collisions with the incident high energy electrons. Thus, at low current, I_γ is proportional to the incident current density, J_b, through the dose rate. At very high current density, saturation can occur when trap states fill, limiting the number of states electrons can decay into, and causing to I_γ to approach a constant value.

Current dependent saturation is shown in Fig. 2, where the spectral radiance as a function of beam current density for various incident beam energies is fit using Eqs. (1) and (2). The departures from the initial linear dependence on current density is attributable to saturation effects at higher current density when trap states fill, limiting the number of states electrons can decay into. This is most pronounced in Fig. 2(a) for the thin sample with a $\dot{D}_{sat}$ value of $4.4 \cdot 10^3 \pm 44\%$ Gy/s. Saturation effects are present, though much reduced, for the thick sample; $\dot{D}_{sat}$ is 577 ± 25% Gy/s in Fig. 2(b). The smaller saturation dose rate for the thicker sample may well be a result of the preparation method for the samples; the vapor deposited thin sample would be expected to have substantially more defects than the thick sample and more defects would require a higher dose rate to produce saturation. Note that as the dose rate changes from thickness-dependent (thin penetrating sample) to range-dependent (thick non-penetrating sample), $\dot{D}_{sat}$ decreases dramatically.

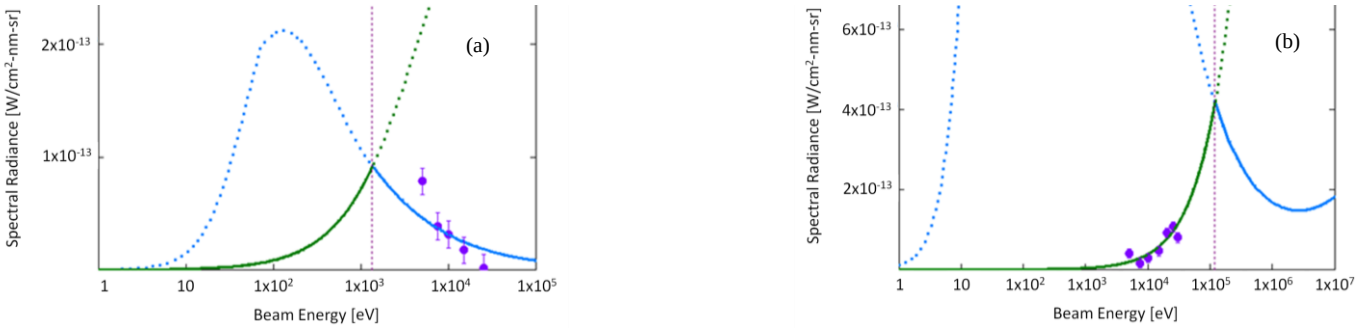

Fig. 3. Spectral radiance relationship with beam energy at 10 nA/cm^2; curves created using the range function and Eqns (1) and (2). The green curve is the behavior of the spectral radiance when the energy dependent range is less than the material thickness; all power is deposited into the sample. The blue curve is the behavior of the spectral radiance when the energy dependent range is greater than the material thickness. The vertical purple dotted line is the energy at which the range is equal to the thickness of the sample, the penetration energy. The luminescent behavior follows the solid portions of the curves. (a) ~60 nm sample; penetration energy ~1.3 keV; range > sample thickness, decreasing with increasing energy. (b) ~80 μm sample; penetration energy ~118 keV; range < sample thickness, increasing with energy.

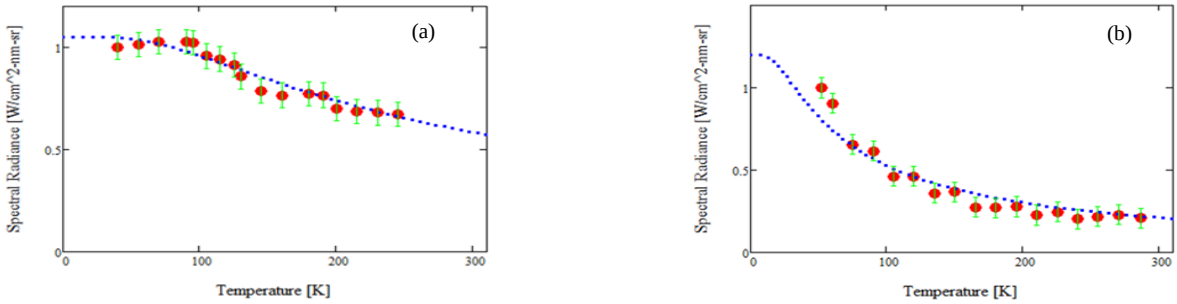

Fig. 4. The spectral radiance of SiO_2 as a function of sample temperature, measured at 5 keV and >200 nA-cm^{-2}. Curves are fit with Eq.(1). (a) 60 nm sample, fit with a ε_{ST} = 21.0±0.5 meV, with a peak temperature of 67 K. (b) 80 µm sample, fit with ε_{ST} = 5.0±0.5 meV, with a peak temperature of 16 K.

B. Incident Beam Energy

Below saturation current densities, I_γ is linearly proportional to $\dot{D}$, as given by Eq. (2). For nonpenetrating radiation, the unsaturated intensity I_γ and $\dot{D}$ are linearly proportional to the incident power density, $(J_b E_b / q_e)$, and to E_b. For penetrating radiation, the unsaturated intensity I_γ scales as $[E_b / R(E_b)]$. The intersection of these two behaviors occurs at the penetration beam energy at which the range, $R(E_b)$, equals the thickness of the sample, L [7]. The expected luminescent behavior follows the solid portions of each curve in Fig. 3 and the dashed curves predict the penetrating and nonpenetrating behavior outside their energy ranges of applicability. The penetration energies are denoted by the purple vertical lines (~1.3 keV for the ~60 nm sample and ~118 keV for the ~80 µm sample). For the thick sample, shown in Fig. 3(b), the maximum beam energy used in the experiments was 30 keV, so the experiments were all nonpenetrating. Measured data (circles) at a constant 10 nA-cm^{-2} shown in Fig. 3 follow the nonpenetrating portion of the predicted curve for the thick sample and the penetrating portion for the thin sample. The fits in Fig. 3 were obtained using the $\dot{D}_{sat}$ value calculated from the previous section related to incident beam current density.

The order of amplitudes of the curves in Fig. 2, increasing amplitudes with increasing energy for the nonpenetrating thick sample in Fig. 2(a) and decreasing amplitudes with increasing energy for the penetrating curves in Fig. 2(b), reflect the energy-dependent behavior described above.

C. Temperature

Figure 4 shows the temperature dependence of the SiO_2 spectral radiance for the two samples measured at 5 keV and >200 nA-cm^{-2}, fit with Eq. (1). As predicted, the spectral radiance of disordered SiO_2 increases exponentially as the temperature decreases until it reaches a maximum intensity value and horizontal asymptote. The minimum energy depth of the occupied ST below the CB, ε_{ST} for the thin sample in Fig. 4(a) is 21.0±0.5 meV and for the thick sample in Fig. 4(b) is 5.0±0.5 meV. The observed differences in ε_{ST} for the two samples (with approximately the same number of electrons excited from the VB) is consistent with the idea that the thicker sample—with a lower defect density due to its fabrication method—would have a effective filling energy closer to ε_{CB}, as trapped electrons collect in the smaller magnitude ST distribution.

D. Emission Spectra and Deep Trap States

Temperature dependent emission spectra in the visible range were also collected for thin and thick samples. The four peaks in the disordered SiO_2 luminescence spectra are attributed to bands of localized defect or "deep trap" (DT) states, at ~1.93, ~2.48, ~2.76, and ~4.97 eV below the CB edge [11]. The raw spectral data were fit with four Gaussian functions to give the spectra shown in Fig. 5. The spectra for the thin sample (Fig. 5(a)) and the thick sample (Fig. 5(b)) both had two dominant bands centered at approximately 500 nm and 645 nm; an additional shoulder was observed at ~455 nm at low temperature (Fig. 5). A fourth peak in the UV range at ~275 nm was observed for the thin samples [11]; the UV range was not measured for the thick sample.

The observed peak positions are consistent with results for similar disordered SiO_2 samples at room temperature [19-24]. Defect origins of some DT states that exist in the electronic band structure of disordered SiO_2, which contribute to CL, have been identified [13,25,26] and are depicted in Fig. 1. The red ~645 nm band is attributed to a nonbridging oxygen hole center (NBOHC) [19,23,24]. The green ~500 nm and UV ~275 nm bands are associated with an oxygen deficient center (ODC) or twofold coordinated silicon centers [20-24].

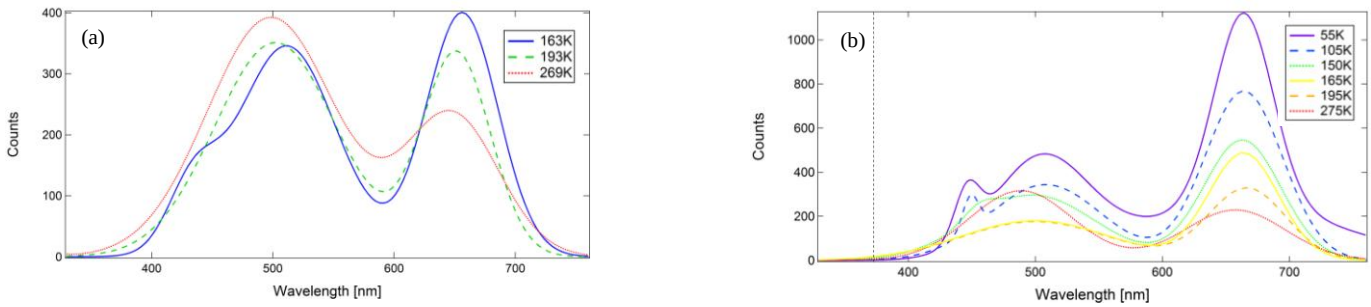

Fig. 5. Fits to measured emission spectra were obtained at various sample temperature. The spectra have two peaks centered at ~500 nm and ~645 nm; an additional shoulder is observed at ~455 nm. (a) Spectra are from the ~60 nm sample, cooled to ~160 K. (b) Spectra from the ~80 µm sample, cooled to ~55 K. No data were measured below ~340 nm (dashed line) for these spectra.

The UV band is attributed to a singlet-singlet (allowed) transition and the green band is attributed to a triplet-singlet (forbidden) transition [23]. The blue ~455 nm band has been tentatively associated with surface defects [22,23].

The intensity of the red, blue and (low T) green bands continually decreased as temperature increased, and are fit well by the overall intensity curve from Eq. (1) [see Fig. 6(a)]. This same peak behavior was also seen in the still camera images, where the red, green and blue components of the color images followed the same temperature dependent trends as the corresponding peaks in the spectra [3,11]. The relative intensities show very consistent temperature behavior for both thick and thin samples. The green band intensities are the exception to these observations. They show similar decrease with increasing temperature up to ~165 K, but then began to increase in intensity somewhat above this temperature [see Fig. 6(a)]. The contrasting behaviors of these peaks are attributed to the thermal dependence of the occupancy of the deep traps; intensity increases with decreasing occupancy [3,8]. The occupancy of different DT—and associated band intensities—are discussed further in Appendix VI.D.

The blue peak intensity is much larger in comparison to the red and green peak intensities, for the thin sample than the thick sample (see Fig. 5). This may reflect an increased contribution of surface effects for the thin sample, consistent with the blue band association with surface defects [22,23].

As temperature changes, the peak widths remain constant [nearly within error bars, see Fig. 6(b)], except in the region where the 455 nm and 500 nm peaks become indistinguishable. Since the depth of the occupied ST is much less than the CB to DT energies ($\varepsilon_{ST} << \varepsilon_{DT}$) and even than the widths of the DT (except the ~455 nm surface state), the width of the emission peaks are largely driven by the width of the deep level trap distributions. The width of the surface defect blue band was 4 to 6 times less than the other three bands attributed to bulk defects (see Table in Fig. 1 and Fig. 6 (b)).

The peak positions of the red, green and blue bands exhibit markedly different temperature behavior [see Fig. 6(c)]. With increasing temperature the red peak shows a very modest decrease in peak position (~1.8 μeV/K), the green and UV peaks show ~4 times greater decrease (~7.6 μeV/K), and the blue peak shows ~4 times greater increase (~8.4 μeV/K). Again, the peak shifts show very consistent behavior for both thick and thin samples. The two peaks attributed to ODC defects (green and UV peaks) exhibit very similar large negative shifts, which differ from the other two peaks attributed to other defects; this suggests that the shifts are largely controlled by the DT defect type. The peak shifts can be explained as due to energy of the emitted photons increasing as the mean occupation level of the DT decreases; this too is related to the occupancy of the DT states as discussed further in Appendix VI.D.

V. Conclusions

Low intensity cathodoluminescence was observed for disordered SiO_2 thin film and bulk samples under low intensity incident electron irradiation. A model based on multilevel disordered peak DOS explains the intensity versus beam current density, beam energy and material temperature trends. As the current density increased, the luminescent intensity increased until it reached a saturation level. Using the model, saturation levels were determined and then used in the energy dependent analysis. When the range was less than the sample thickness, at sufficiently low energy beam, the luminescent intensity increased linearly with energy. However, once the range exceeded the sample thickness, the intensity fell off with increasing energy. The model also extends to the temperature dependent behavior of cathodoluminescence. After initially increasing with decreasing temperature, the overall intensity approaches a horizontal asymptote. The temperature dependence of the individual bands largely followed the same temperature behavior as the overall intensity. The observed number and wavelengths of the peaks were consistent with previous observations. The intensity and peak positions of the primary peaks observed in the visible region were measured as a function of temperature from ~55 K to ~280 K. Using these fits from the model, the material and sample properties relating to the defect density of states, $\dot{D}_{sat}$ and ε_{ST}, were determined.

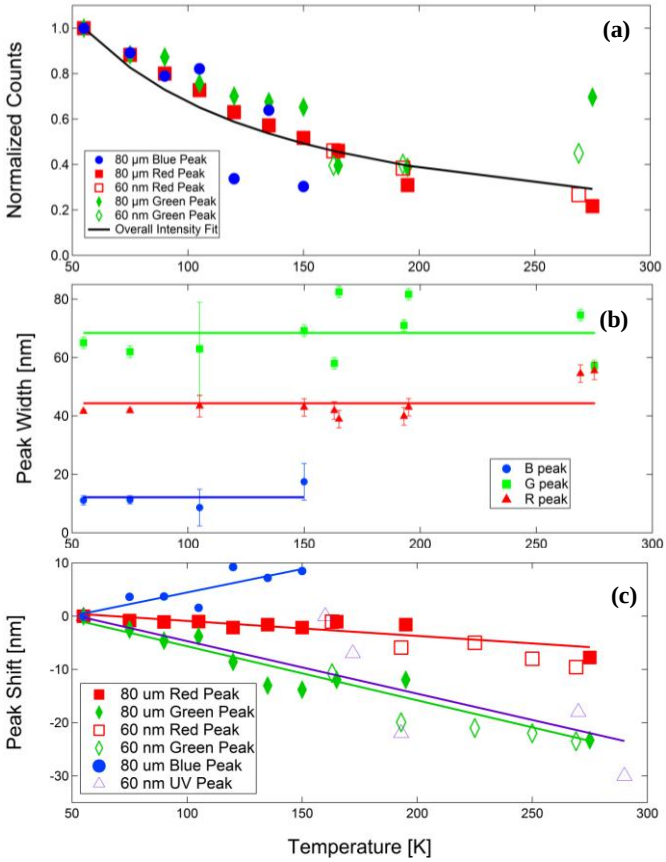

Fig. 6. (a) Temperature dependence of spectral peaks, normalized to the most intense low temperature peak value. Fit is for overall intensity data based on Eq. (1). (b) Temperature dependence of the peak widths, with mean values shown. (c) Temperature dependence of the peak positions with linear fits. Data are for ~650 nm red (squares), ~500 nm green (diamonds), ~455 nm blue (circles) , and ~275 nm UV (triangles) peaks. Separate values are shown for the thin (open symbols) and thick (solid symbols) data.

Results of these experiments suggest that materials used in structural components, optical elements, and thermal control surfaces of spacecraft and space-based observatories could—when exposed to sufficiently energetic, charged particles from the space plasma environment—luminesce [9,11,17,24,27]. If these visible, infrared and ultraviolet emissions are intense

enough, they could potentially produce optical contamination detrimental to the performance of a spacecraft's optical elements and sensors, and act to limit their sensitivity and performance windows [28]. Alternately, cathodoluminescence could be used to observe and characterize spacecraft under intense electron bombardment [29]. By extending its application to other types of materials [17], this model becomes an integral component in understanding the affects of the space environment on many types of spacecraft.

VI. Appendix

Equation (1) for the luminescent intensity, I_γ, can be extended to include further details of the intrinsic and extrinsic material properties and the deep level states.

A. Range and Sample Thickness

Assuming normal incidence electrons and a constant stopping (constant slow-down approximation, CSDA [16]), the final depth-dependent term in curly brackets in Eq. (1) from the upward emitting hemisphere of photons is

$$\int_o^{R(E_b)} dz\ \Theta[L-z] \int_1^0 d(\cos(\theta)) = \begin{cases} R(E_b)\ ;\ 0 \le R(E_b) \le L, & \text{nonpenetrating} \\ L\ ;\ 0 \le L \le R(E_b), & \text{penetrating} \end{cases} . \quad (3)$$

for an abrupt end of the luminescent sample at depth L. The result is the same for either normal or isotropic photon emission at the point of luminescence.

B. Reflectivity at Interface

The model of an interface at L can be extended by considering non-zero wavelength-dependent reflectivity of the emitted photons, $\mathbb{R}_m(\lambda)$. This could describe reflective mirror coating considered in [30] or changes in the index of refraction at the interface [31]. This adds a multiplicative term $\frac{1}{2}[1+\mathbb{R}_m(\lambda)]$ to Eq. (1). This is the same for either normal or isotropic photon emission with no absorption by the material, since all photons will eventually exit the sample. For highly reflective materials like Ag, $\mathbb{R}_m \approx 1$ at all λ considered. For materials like Au, the emission spectrum is enhanced at longer λ, due to lower reflectivity of Au at shorter λ.

C. Material Absorption

For absorptive materials, characterized by a wavelength-dependent absorption coefficient, α(λ), Eq. (3) becomes

$$\int_o^{R(E_b)} dz\,\Theta[L-z] \int_1^0 d(\cos(\theta)) \times \left[e^{-\alpha(\lambda)\cdot z} + \mathbb{R}_m(\lambda) e^{-\alpha(\lambda)\cdot(2L-z)}\right] = \frac{1}{2\alpha(\lambda)} \begin{cases} \left(1-e^{-\alpha(\lambda)\cdot R(E_b)}\right)\left[1+\mathbb{R}_m(\lambda)e^{-\alpha(\lambda)\cdot L}e^{-\alpha(\lambda)\cdot(L-R(E_b))}\right] \\ \left(1-e^{-\alpha(\lambda)\cdot L}\right)\ \left[1+\mathbb{R}_m(\lambda)e^{-\alpha(\lambda)\cdot L}\right] \end{cases} . \quad (4)$$

The first and second terms in square brackets of Eq. (4) correspond to normal photon emission from the upward and downward emitting hemispheres, respectively. To account for isotropic photon emission, *z* in these two terms is replaced by *z/cos(θ)*. The overall emission is reduced for the longer non-normal path lengths at higher angles; however, this is a small effect as long as attenuation through the material is small, *i.e.*, $\alpha(\lambda)\cdot L<1$. The optical absorption is small for propagation through the SiO_2 coating films considered here; thus it does not contribute significantly for these measurements.

D. Final Deep Trap State Dependence

The relative intensities of individual bands is described in Eq. (1) through the relative conversion efficiency of excited electrons to photons from each band, $Q_{e\gamma}(\lambda,T)$. This depends in complex ways on:

(i) the energy and spatial distributions of defects in the different DT states,
(ii) the type of defects through the transition rates from ST states to different DT states [25,26], and
(iii) the number of *available* DT states.

The integrated peak intensities for disordered materials are roughly proportional to the density of states for the associated defect, since there are no symmetry selection rules for disordered states [13]. Further, the spectrometer response function is relatively flat over the spectral range shown in Fig. 5, so the peak widths are reasonable measures of the DT distribution widths. The peaks were found to be fit best with symmetric Gaussian line shapes, rather than asymmetric Lorentzian or Voigt line shapes; this would be expected for ST and DT states with long life times and corresponding small lifetime broadening [9,14].

The relative intensities of individual bands are also proportional to the number of available DT states, which can have significant temperature dependence. For a given disordered band this is often characterized by the effective Fermi level (EFL, the level within each band at which occupation reaches 50%); [13] and [26] discuss the behavior of the EFL and corresponding temperate dependence of intensities for different types of defects observed in amorphous SiO_2. The equilibrium EFL can decrease (move towards the CB, as measured from the CB edge) with increasing stored charge as DT are filled, due for example to increased dose rate or decreased conductivity. (An informative test—similar to those described in Sec. IV.D— would be to observe the shift of peak positions with increased charge accumulation or surface voltage under prolonged beam exposure.) The EFL can also decrease with decreasing temperature as fewer electrons in the DT can be thermally excited from the traps, as described in [12]. However, thermal excitation out of DT with binding energies >1.9 eV and into ST or the CB is highly improbable at room temperature and below. Hence, both stored charge and thermal excitation into ST or the CB should act similarly for all DT and not lead to significant addition temperature dependence of the intensities. Thermal excitation from one DT to another is also unlikely, due to minimal spatial overlap of the two localized states [13].

Another mechanism that affects the EFL is the rate at which DT are emptied by non-radiative processes. Non-radiative processes (for example, multiple phonon, plasmon or polaron processes) relaxing DT electrons directly to VB, low level hole traps or lower energy DT can increase the overall number of DT available for radiative luminescence and the concomitant overall intensity [13,25]. In general, these are expected to be infrequent and have weak temperature dependence due to the large bandgap in SiO_2. However, transitions from deeper DT requiring creation of fewer

quasiparticles are more likely than transitions from shallower DT. The observed increase in green band intensity with increasing temperature [see limited data in Fig. 6(a)] is fit reasonably well with an empirical model $I_\gamma \propto \left[1 - e^{-(\varepsilon_{ST}/k_B T)}\right] \cdot e^{-(n_{QP}\varepsilon_{QP}/k_B T)}$ with $n_{QP}\cdot\varepsilon_{QP}\approx$20 meV, where ε_{QP} can be interpreted as the energy required to create a quasiparticle and n_{QP} as the number of quasiparticles created in a transition from a DT to lower energy states.

ACKNOWLEDGEMENT

We acknowledge Michael Taylor for the use of infrared and CCD video cameras, and useful discussions with Robert Meloy and Charles Bowers of NASA Goddard Space Flight Center. We are also grateful for contributions of members of the Materials Physics Group, especially Justin Dekany, Greg Wilson, and Tamara Jeppsen.

REFERENCES

[1] D. Hastings and H. Garrett, *Spacecraft-Environment Interactions*. New York, NY: Cambridge Press, 1996.

[2] R. Leach and M. Alexander, "Failures and anomalies attributed to spacecraft charging," *NASA STI/Recon Technical Report N*, vol. 96, p. 11547, 1995.

[3] A.E. Jensen and J.R. Dennison, "Defects Density of States Model of Cathodoluminescent Intensity and Spectra of Disordered SiO_2," in *Proc. 13th Spacecraft Charging Tech. Conf.*, Pasadena, CA, 2014.

[4] W. Y. Chang, J. R. Dennison, N. Nickles, and R. E. Davies, "Utah State University Ground-based Test Facility for Study of Electronic Properties of Spacecraft Materials," in *Proc. 6th Spacecraft Charging Tech. Conf.* Hanscom Air Force Base, MA, 1998.

[5] J. Dekany, R. H. Johnson, G. Wilson, A. Evans, and J. R. Dennison, "Ultrahigh Vacuum Cryosat System for Extended Low Temperature Space Environment Testing," *IEEE Trans. on Plasma Sci*, vol. 42, pp. 266-271, 2014.

[6] W. Y. Chang, J. Dennison, N. Nickles, and R. E. Davies, "Utah State University Ground-based Test Facility for Study of Electronic Properties of Spacecraft Materials," in *Proc. 6th Spacecraft Charging and Technology Conference*, Hanscom Air Force Base, MA, 2000.

[7] G. Wilson, "The Internal Charge Evolution of Multilayered Dielectrics Undergoing Mono-Energetic Electron Bombardment," MS Thesis, Physics Dept., Utah State Univ., Logan, UT, 2015.

[8] J. R. Dennison, A. Evans, G. Wilson, C. W. Bowers, and R. Meloy, "Electron Beam Induced Luminescence of SiO_2 Optical Coatings," in *Conference on Electrical Insulation and Dielectric Phenomena* Montreal, Canada, 2012.

[9] A.E. Jensen, "Space Plasma Environment Induced Luminescence of Materials on Space Based Observatories," MS Thesis, Physics Dept., Utah State Univ., Logan, UT, 2014.

[10] JR Dennison, J. Gillespie, J.L. Hodges, R.C. Hoffmann, J. Abbott, A.W. Hunt and R. Spalding, "Radiation Induced Conductivity of Highly-Insulating Spacecraft Materials," in Appl. of Accelerators in Res. and Industry, *Am. Inst. Phys. Conf. Proc. Ser.*, vol. 1099, ed. F.D. McDaniel and B.L. Doyle, (Am. Inst. Phys., Melville, NY, 2009), pp. 203-208.

[11] A. E. Jensen, G. Wilson, J. Dekany, A. Sim, and J. R. Dennison, "Low Temperature Cathodoluminescence of Space Observatory Materials," *IEEE Trans. on Plasma Sci*, vol. 42, pp. 305-310, 2014.

[12] J. R. Dennison, J. Dekany, J. C. Gillespie, P. Lundgreen, A. Anderson, A. E. Jensen, G. Wilson, A. Sim, and R. Hoffman, "Synergistic models of electron emission and transport measurements of disordered SiO_2," in *Proc. 13th Spacecraft Charging Tech. Conf.*, Pasadena, CA, 2014.

[13] S.R. Elliot, *Physics of Amorphous Materials*. 2nd Ed., New York, NY: Longman Scientific and Technical, 1990.

[14] J.R. Lakowicz, "Principles of Flourescnece Spectroscopy," New York, NY: *Plenum Press*, 1983.

[15] A. Joblonski, "Uber den Mechanismmus des Photolumineszenz von Farbstoffphosphoren," Z. Phys., vol. 94, no. 1-2, pp. 38–46, 1935.

[16] G. Wilson and J. R. Dennison, "Approximation of Range in Materials as a Function of Incident Electron Energy," *IEEE Trans. on Plasma Sci*, vol. 40, pp. 291-297, 2012.

[17] J. Dekany, J. Christensen, J. R. Dennison, A. E. Jensen, G. Wilson, T. Schneider, C. W. Bowers, and R. H. Meloy, "Variations in cathodoluminescent intensity of spacecraft materials exposed to energetic electron bombardment," *IEEE Trans. on Plasma Sci*, 2015, in press.

[18] M.J. Treadaway, B.C. Passenheim, and B.D. Kitterer, "Luminescence and Absorption of Electron-Irradiated Common Optical Glasses, Sapphire, and Quartz," *IEEE Trans. Nuc. Sci.*, Vol. NS-22, No. 6, 2253-2258, 1975.

[19] R. Salh, A. v. Czarnowski, M. V. Zamoryanskaya, E. V. Kolesnikova, and H. J. Fitting, "Cathodoluminescence of SiO_x under-stoichiometric silica layers," *Physica Status Solidi (a)*, vol. 203, pp. 2049-2057, 2006.

[20] A. N. Trukhin, M. Goldberg, J. Jansons, H. J. Fitting, and I. A. Tale, "Silicon dioxide thin film luminescence in comparison with bulk silica," *J.Non-Crystalline Solids*, vol. 223, pp. 114-122, 1998.

[21] S.W. McKnight, and E.D. Palik, "Cathodolumine-scence of SiO_2 Films," *J. Non-Crystalline Solids*, vol. 40, pp. 595, 1980.

[22] J.P. Mitchell, and D.G. Denure, "A Study of SiO Layers on Si Using Cathodoluminescence Spectra," *Solid-State Electronics*, vol. 16, p. 825, 1973.

[23] M. Goldberg, H.J. Fitting and A.N. Trukhin, "Cathodoluminescence and Cathodoelectroluminescence of Amorphous SiO_2 Films," *J. Non-Crystalline Solids* vol. 220, p. 69, 1997.

[24] H. J. Fitting, T. Barfels, A. N. Trukhin, and B. Schmidt, "Cathodoluminescence of crystalline and amorphous SiO_2 and GeO_2," *J. Non-Crystalline Solids*, vol. 279, pp. 51-59, 2001.

[25] R.A. Street, in *Semiconductors and Semimetals*. J. Pankove, Ed., vol. 21B. New York, NY: Academic, 1984.

[26] J. Robertson, The Physics and Technology of Amorphous SiO_2. R.A.B. Devive, Ed., New York, NY: Plenum, 1988.

[27] V. Griseri, L. A. Dissado, J. C. Fothergill, C. Laurent, and G. Teyssedre, "Photoluminescence, recombination induced luminescence and electroluminescence in epoxy resin," *J. Physics D: Applied Physics*, vol. 34, 2001.

[28] J.R. Dennison, A.E. Jensen, J. Dekany, G. Wilson, C.W. Bowers and R. Meloy, "Diverse Electron-induced Optical Emissions from Space Observatory Materials at Low Temperatures," *Proc. SPIE Cryogenic Optical Systems and Instr. Conf.*, Vol. 8863, 2013, pp. 88630B1-88630B15.

[29] D. C. Ferguson, J. Murray-Krezan, D.A. Barton J.R. Dennison, and S. Gregory, "Feasibility of Detecting Spacecraft Charging and Arcing by Remote Sensing," *J. Spacecraft and Rockets*, vol. 51, no. 6, pp. 1907-1913, 2014.

[30] A.E. Jensen, J.R. Dennison, G. Wilson, J. Dekany, C.W. Bowers, R. Meloy and J.B. Heaney, "Properties of Cathodoluminescence for Cryogenic Applications of SiO_2-based Space Observatory Optics and Coatings," *Proc. SPIE Cryogenic Optical Systems and Instr. Conf.*, Vol. 8863, 2013, pp. 88630A1-88630A10.

[31] A. Evans and J.R. Dennison, "The Effects of Surface Modification on Spacecraft Charging Parameters," *IEEE Trans. on Plasma Sci*, vol. 40, pp. 291-297, 2012. .

Amberly Evans Jensen received BS degrees in physics and chemistry in 2012 and an MS degree in physics in 2014 all from Utah State University in Logan, UT. She has worked with the Materials Physics Group for seven years studying electron emission, luminescence, and resistivity and the retrieval and postflight analysis of *SUSpECS* samples from the MISSE-6 project. Much of her work has focused on optical scattering and emission of spacecraft materials.

J. R. Dennison (M '12) received the B.S. degree in physics from Appalachian State University, Boone, NC, in 1980, and M.S. and Ph.D. degrees in physics from Virginia Tech, Blacksburg, in 1983 and 1985, respectively. He was a Research Associate with the University of Missouri—Columbia before moving to Utah State University (USU), Logan, UT in 1988. He is currently a Professor of physics at USU, where he leads the Materials Physics Group. He has worked in the area of electron scattering for his entire career and has focused on the electron emission and conductivity of materials related to spacecraft charging for the last two decades.